IOP Publishing J. Phys. Energy 5 (2023) 035011 https://doi.org/10.1088/2515-7655/ace7f5

Journal of Physics: Energy

OPEN ACCESS

RECEIVED
13 May 2023

REVISED
6 July 2023

ACCEPTED FOR PUBLICATION
17 July 2023

PUBLISHED
2 August 2023

PAPER

Controlled assembly of perovskite nanoparticles by photoswitchable functional ligands

Tal Binyamin, Orit Cohen, Idan Cohen and Lioz Etgar*

The Hebrew University of Jerusalem, Institute of Chemistry, Casali Center for Applied Chemistry, Jerusalem, Israel
* Author to whom any correspondence should be addressed.

E-mail: lioz.etgar@mail.huji.ac.il

Keywords: controlled, assembly, perovskites, nanoparticles, photoswitchable, functional

Supplementary material for this article is available online

Abstract

Organic ligands play a crucial role in the properties and functionality of nanostructures. Functional ligands are an interesting research direction that can be utilized to influence the properties and functionality of nanoparticles (NPs). In this work, we demonstrate controlled assembly of $CsPbBr_3$ perovskite NPs as a result of light. Azobenzene derivative molecules were used as the photoswitchable ligands for the NPs. The assembly and disassembly of the NPs were achieved by *cis–trans* isomerization. By utilizing polarization-modulated, infrared reflection–absorption spectroscopy and diffusion-ordered nuclear magnetic resonance, we were able to track the attachment of the ligands to the surface of the NPs. Absorbance, photoluminescence and high-resolution, transmission electron microscopy followed the assembly and disassembly of the NPs. This work demonstrates functional ligands paired to perovskite nanostructures through controlling their assembly and disassembly, which opens the way for sensing and photodetection applications.

1. Introduction

Due to their remarkable optical and physical properties, perovskite nanoparticles (PeNPs) have been intensively investigated in recent years. PeNPs are characterized by a high photoluminescence (PL) quantum yield, narrow full width at half maximum (FWHM) of emission, and tunable band gap [1]. These properties enable PeNPs to be used in light-emitting diodes [2–4], lasers [5, 6], sensors [7, 8], and photodetectors [9, 10]. The ligands in PeNPs form an organic shell that plays a crucial role and affects the physical and optical properties of the NPs [11, 12]. The organic shell is composed of oleic acid (OA) and oleylamine (OLA). Substitution of the ligands can increase the stability of the NPs under humidity, improve optical properties, and stabilize the composition of the perovskite [13–15]. One more interesting pathway is using ligands with specific functionality that influences the properties of the NPs. For example, chiral molecules can act as ligands to the NPs, which enables the application of circularity-polarized, photodetector-based PeNPs [16–18]. Another option is to use switchable molecules as the ligands for the PeNPs. Photoswitchable molecules are chromophores that change their physical properties as a result of light. Azobenzene and stilbene derivatives act as good photoswitches; the polarity of the molecules changes during the *cis–trans* isomerization, resulting in a decrease in solubility and formation of aggregates of the molecules [19]. When using these photoswitchable molecules as ligands for NPs, they can influence the assembly and disassembly of the NPs. The use of photoswitchable molecules as ligands for gold (Au) NPs was reported by Klajn *et al* [20]. Klajn *et al* and a few later studies showed the controlled assembly of Au NPs as a result of light, with different photoswitchable ligands [21, 22]. Moreover, previous studies have demonstrated that the isomerization process of functional ligands can change the catalytic activity of the NPs [23–28]. Here, we demonstrate for the first time controlled assembly of PeNPs due to a reaction with light. The process is based on the isomerization of 4-[4-(2-Phenyldiazenyl)phenoxy]butanoic acid (PDPB) ligands (i.e., azo ligands).

We synthesized PDPB molecules with carboxylic acid in order to attach them to the surface of the PeNPs. The polarity of the ligands was changed as a result of the isomerization reaction; the *cis* molecule carried dipole moment as opposed to the *trans* molecule, which was nonpolar. The polarity of the PeNPs changed accordingly and affected the assembly process. The ligand exchange process was studied by following the changes in the optical properties of the PeNPs and by diffusion-ordered NMR spectroscopy (DOSY-NMR). Furthermore, we used dynamic light scattering (DLS) and high-resolution, transmission electron microscopy (HR-TEM) to follow the assembly process. In addition, due to the possibility of controlling the distance between the NPs, we were able to switch on and off an energy transfer process between the NPs.

2. Methods

Cesium carbonate (Cs_2CO_3, 99.9%, Sigma-Aldrich), lead(II) bromide ($PbBr_2$, ⩾98%, Sigma-Aldrich), lead(II) oxide (PbO, ⩾99.0%, Sigma-Aldrich), hexamethyldisilathiane (TMS_2S, Sigma-Aldrich), aniline (⩾99.5%, Sigma-Aldrich), phenol (99.0%–100.5%, Sigma-Aldrich), sodium nitrite (⩾99%, Sigma-Aldrich), potassium carbonate, sodium hydroxide (NaOH, ⩾98%, Sigma-Aldrich), ethyl 4-bromobutanoate (95%, Apollo Scientific), hydrochloric acid (37%, Sigma-Aldrich), OA (90%, Sigma-Aldrich), OLA (70%, Sigma-Aldrich), 1-octadecene (ODE, 90%, Sigma-Aldrich), ethyl acetate (⩾99.5%, Sigma-Aldrich), hexane (96%, DAEJUNG), toluene (99.7%, DAEJUNG), and acetone AR (CARLO HRBA) were purchased and used as received without any further purification.

2.1. Synthesis of azo ligands

The PDPB was synthesized following the procedure of Renier *et al* [29] for similar products. First, three solutions were prepared: (1) 0.05 mol of Aniline was dissolved in 50 ml HCl (3 M) in a round bottom flask; (2) 0.05 mol of $NaNO_2$ was dissolved in 10 ml of water; and (3) 0.05 mol of phenol was dissolved in 25 ml of NaOH (10% in water). Solutions 1 and 3 were cooled to a temperature below 5 °C. Then, the solutions, first Solution 2 and then Solution 3, were added dropwise to Solution 1 in the flask while maintaining a low temperature. The orange precipitate was collected and rinsed with water until the water filtrated was neutralized, and the product was dried under vacuum overnight (72% yield). In the next step, the previous product was mixed with K_2CO_3 and ethyl 4-bromobutanoate (E4B) in a ratio of 1:1:2, respectively, and dissolved in 20 ml of acetone and refluxed for 24 h. The solids were separated from the liquid by Buchner. Then, the supernatant was dried under vacuum to extract the solid product, which was rinsed with hexane and recrystallized from ethanol (60% yield). The final step was ester hydrolysis to form the carboxylic compound. About 10 mmol of the previous product was dissolved in 50 ml of ethanol and 50 ml of NaOH (25% w/w in water) and refluxed overnight. The ethanol was removed by evaporation, and HCl was added to the crude solution to induce the precipitation of the product. The yellow-orange solid was dried under vacuum overnight. The orange solid was recrystallized from ethanol (87% yield) for further use. The product was analyzed by H-NMR in DMSO-d to verify the final product according to a report by Müller *et al* [30]. Benzene d6 was used for the analysis of the interaction between the PeNPs and ligands. H-NMR was at (400 MHz, benzene-d6, and δ (ppm)): 8.065 (ArH, 4H), 7.215 (ArH, 3H), 6.721 (ArH, 2H), 3.414 (O$\mathbf{CH_2}$, 2H), 2.172 ($\mathbf{CH_2}$COOH, 2H), and 1.724 ($OCH_2\mathbf{CH_2}CH_2COOH$).

2.2. Preparation of Cs-oleate

The Cs-oleate precursor was prepared according to a previously published procedure by Protesescu *et al* and by us [1]. In a 100 ml three-neck flask, 1.228 mmol of Cs_2CO_3 was mixed with 625 μl of OA and 7.5 ml of ODE. The solution was degassed for 1 h under vacuum conditions at 120 °C and then heated to 150 °C under argon flow.

2.3. Synthesis of $CsPbBr_3$ NPs

The NPs were synthesized by the hot injection method. First, 0.188 mmol of $PbBr_2$ was mixed with 0.5 ml of OA, 0.5 ml of OLA, and 5 ml of ODE in an additional 100 ml three-neck flask. The solution was degassed for 1 h under vacuum at 120 °C and then heated to 150 °C under argon flow. The reaction was carried out by injecting 0.4 ml of the Cs-oleate precursor solution into the $PbBr_2$ precursor solution using a syringe. The reaction was quenched using an ice bath after a few seconds. Ethyl acetate was added to the crude solution in a volume ratio of 3:1 and the NCs were centrifuged at 6000 rpm for 10 min and the participate was dispersed in toluene. The cleaning process was repeated twice. The purified NCs were dispersed in toluene for further use.

2.4. Ligand exchange

The amount of 50 μl of $CsPbBr_3$ in toluene (50 mg ml^{-1}) was added to the ligand solutions (2–6 mg in 1 ml of toluene) and stirred overnight. The azo-capped NPs were extracted by centrifugation at 6000 rpm for 10 min and dispersed in toluene for further characterization.

2.5. HR-TEM

The morphologies of the NPs were analyzed with a HR-TEM Tecnai F20 G2 (FEI Company, USA). Samples were prepared as follows: 2.5 μl of the NPs dispersion were dropped on an ultralight copper grid coated with amorphous carbon film.

2.6. Optical measurements

Absorbance spectra were recorded using a Jasco V-670 spectrophotometer. PL and the PL lifetimes were measured with a Horiba Scientific Fluoromax-4 spectrofluorometer. For PL measurements, the NPs were excited at 350 nm.

2.7. Polarization–modulation infrared reflection absorption spectroscopy (PM-IRRAS) measurement

PM-IRRAS measurements were performed with PMA-50 coupled to a Vertex 70 Bruker spectrometer at room temperature and under a nitrogen atmosphere in a reflection–absorption cell (Harrick, Inc.). Approximately 2048 scans were performed with a resolution of 4 cm^{-1} while using a mercury–cadmium–telluride detector.

2.8. NMR measurement

H-NMR spectra were measured at 400.13 MHz on a Bruker AMX 400 spectrometer using benzene-d_6 (δ7.15) with chloroform as an internal standard (δ6.15). DOSY-NMR spectra were measured at 500.30 MHz on a Bruker AMX 500 spectrometer using benzene-d_6 (δ7.15).Sample preparation: The free ligands were dispersed in the d-NMR solvent directly, and then the same solution was added to pre-dry PeNPs and stirred overnight, and measured again to track the changes.

2.9. DLS measurement

DLS measurements were conducted with Nanosizer Nano S (Malvern Instruments, Malvern, UK) at room temperature. Each measurement was repeated 3 times with 12 cycles.

3. Results and discussion

We synthesized PDPB ligands (i.e., azo ligands) that underwent an isomerization reaction from *trans* (E)-PDPB to *cis* (Z)-PDPB upon excitation at certain wavelengths. Figure 1(a) presents a schematic illustration of the *cis–trans* isomerization, and the wavelengths required for each reaction. The isomers were characterized with different absorbance curves due to different dominant transitions. While both contain π-π^* and n-π^* transitions, the *trans* was characterized with π-π^* and the *cis* with a n-π^* transition. The *trans* was the thermodynamically stable isomer, while its main peak had a π-π^* transition [31, 32]. Once it was switched from *trans* to *cis* isomerization, the polarity of the molecule changed; from a nonpolar molecule (*trans* isomer) to a polar molecule with dipole moment (*cis* isomer) [33]. The polarity affected the solubility of the ligands in nonpolar solvents; therefore, the solubility of the ligand decreased with the *trans* to *cis* transition. As a result, the *trans* isomer stabilized the NPs in nonpolar solvents. When switching to the *cis* isomer, the polarity changed and the ligands remained attached to the NP's surface thereby preventing coagulation; this provided controlled assembly of the NPs in nonpolar solvents.

Figure 1(b) shows the absorbance spectra of the ligands in both *cis* and *trans* upon excitation. The difference in the absorbance can be clearly observed for the two isomers. Figure 1(c) presents the absorbance and PL of the PeNPs with the original ligands. OA and OLA, in which the absorbance of the PeNPs with the azo ligands before and after excitation by the 365 nm wavelength, are shown in figure 1(d). The change from *trans* to *cis* can be observed due to the decrease in the π-π^* peak. The presence of the PeNPs can also be recognized in the absorbance spectra in figure 1(d) due to the onset at the 520 nm wavelength (inset in figure 1(d)). XRD measurements of the PeNPs before and after the ligands exchange indicate that the PeNPs did not go any phase transfer during the process (figure 1S in the supporting information-SI). In order to study in more detail the ligand exchange process, the concentration of the azo ligands added to the PeNP solution was changed. Figure 2(a) presents the absorbance of the azo ligands and PeNPs at different concentrations of ligands in the solution. As the concentration of the ligands increased from 2 to 8 mg ml^{-1}, the absorbance peak n-π^* increased significantly. Although it may be suggested that the affinity of the ligands to the surface of the NPs increased at high concentrations, the absorbance peak of the PeNPs became weaker when increasing the ligand concentration. This can be explained due to the screening of the n-π^* band and

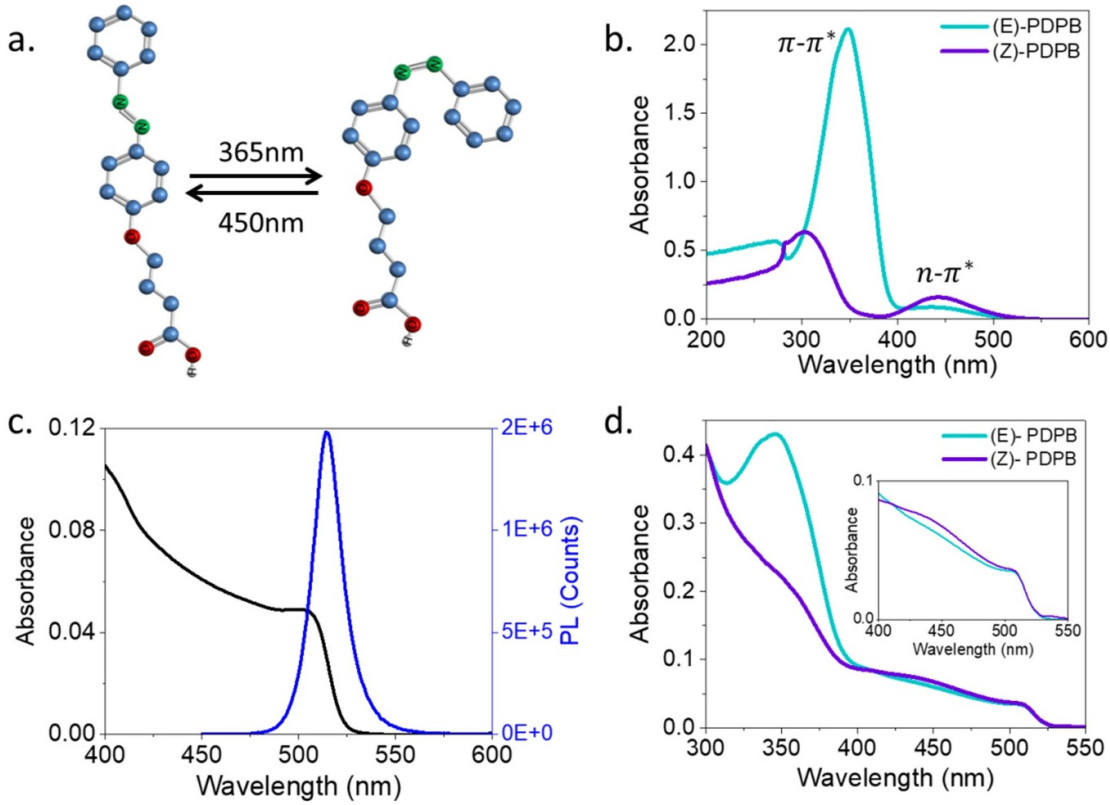

Figure 1. (a) *Cis–trans* isomerization reaction of the molecule 4-[2-(phenylcarbamoyl)phenoxy] butanoic acid. (b) Absorbance spectra of the *cis* and *trans* isomers. (c) Absorbance and photoluminescence spectra of $CsPbBr_3$ PeNPs with the original ligands. (d) Absorbance of $CsPbBr_3$ PeNPs capped with *cis* and *trans* azo ligands.

by the fact that less PeNPs participated in the ligand exchange reaction (changes in the PeNP environment and excess of OLA and OA affected their stability and dispersity) [34, 35]. Therefore, to observe a more complete picture of this situation, we conducted PL measurements at various concentrations, which showed that the PeNP PL intensity decreased with the increase in ligand concentration (figure 2S). Based on these results, we decided to use a concentration of 5 mg ml^{-1} of azo ligands during the remainder of this work, as discussed below. The high absorbance coefficient of the PDPB molecule enables to study the ligand exchange efficiency; the concentration of the ligands in the initial solution should decrease after the ligands exchange process. The ligands which interact with the PeNPs will be removed from the solution during the separation of the NPs which indicate on the ligands exchange efficiency. The concentration of the ligands can be calculated from their absorbance using Beer–Lambert's law, $A = l\varepsilon C$ (where A is absorbance, C is concentration and ε is the absorption coefficient, l the optical way). The azo-ligands were measured at different concentration and tracked at their absorbance wavelength (348 nm). The absorption coefficient is extracted from the slope of the Beer–Lambert's graph which was equal to $\varepsilon = 18\,530\ cm^{-1}M^{-1}$ (see figure 3S in SI). Using ε it is possible to calculate the ligand's concentration in the solution before and after the ligands exchange process. The ligand's concentration was reduced by ∼20% from the initial concentration.

In order to investigate the ligand attachment to the PeNPs, we used PM-IRRAS FTIR. PM-IRRAS was used to measure the pure azo ligands and the PeNPs capped with the azo ligands. The results are presented in figure 2(b). The main differences were the reduction in the peak of O–H bending of carboxylic acid at 1440 cm^{-1} and the appearance of the carboxylate ion peak at 1538 cm^{-1} [36]. In order to interact with the NPs, the azo ligands should have undergone acid–base reactions to form the carboxylate ion. These results suggest that the azo ligands interacted with OLA in acid–base reactions; therefore, the three ligands could interact with the PeNP surface. Below a 1050 cm^{-1} wavenumber, the peaks were related to C=C alkene bending of OA and OLA, while at a 1250 cm^{-1} wavenumber, the C–N stretching of the OLA could be observed. The stretching of the aromatic C=C bond of the azo (PDPB) could be seen at a 1598 cm^{-1} wavenumber, and the carbonyl stretching was located at a 1702 cm^{-1} wavenumber for both the azo ligands and OA.

To further study the interactions between azo ligands and PeNPs, H^1 nuclear magnetic resonance (H-NMR) measurements were performed. Figure 2(c) shows the H-NMR spectra of the pure azo ligands and

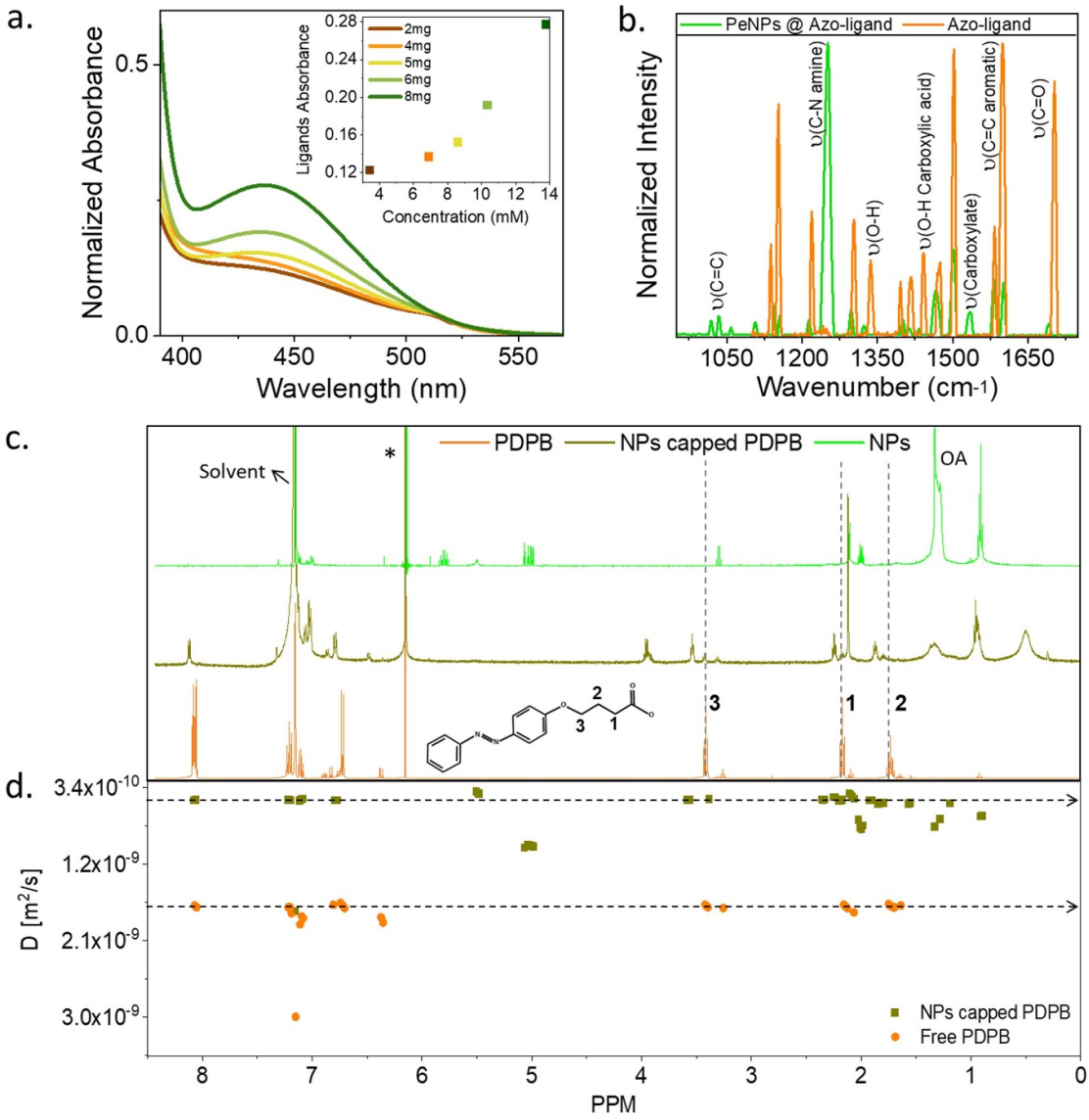

Figure 2. (a) Absorbance of PeNPs capped with azo ligands treated with different ligand concentrations varying between 2 and 8 mg ml^{-1}. Inset: absorbance intensity versus the concentration of the ligands. (b) PM-IRRAS FTIR spectra of the azo ligands and the PeNPs capped with the azo ligands. (c) H-NMR of the azo ligands (orange), the PeNPs capped with the azo ligands (brown), and the pure PeNPs (green), where '*' is the signal of the internal standard (chloroform) in benzene-d6. (d) DOSY-NMR of the free azo-ligands (orange), compared to the azo-ligands attached to the PeNPs (brown) in benzene-d6.

the azo ligands attached to the PeNPs in benzene d6. We used chloroform as an internal standard in order to follow the changes in the azo ligand peaks. Comparing the H-NMR spectra of both cases indicates the changes in the signals of the hydrogens on 1, 2, and 3 carbons (which are the closest to the binding site; see inset in figure 2(c)) toward higher chemical shifts after the addition of the PeNPs. These chemical shifts were due to environmental changes that occurred after the binding of the ligands. Furthermore, the peak integration of the ligands decreased after the addition of the PeNPs, indicating ligand exchange (at 8.0 ppm, 7.2 ppm and 3.4 ppm; the full spectra can be found in figure 4S). This observation indicates that the azo ligands have the ability to attach to the surface of the NPs together with the original ligands which are pronounced as well in the spectrum [11]. Moreover, we performed DOSY-NMR in order to study the differences in the diffusion of the attached azo-ligands, compared to the free Azo-ligands (see figure 2(d)). The measured diffusion coefficient of the free Azo-ligands was 1.7^{-9} (m^2 s^{-1}) while the attached Azo-ligands show diffusion coefficient of 4.9^{-10} (m^2 s^{-1}) which is slower by one order of magnitude. The diffusion coefficient of the bound ligands are similar to the diffusion coefficient of the PeNPs which determined by the common ligands (based on the DOSY-NMR signals). The signals with higher diffusion coefficient can be related to the detached ligands. The difference in the diffusion coefficients supports the ligands exchange process.

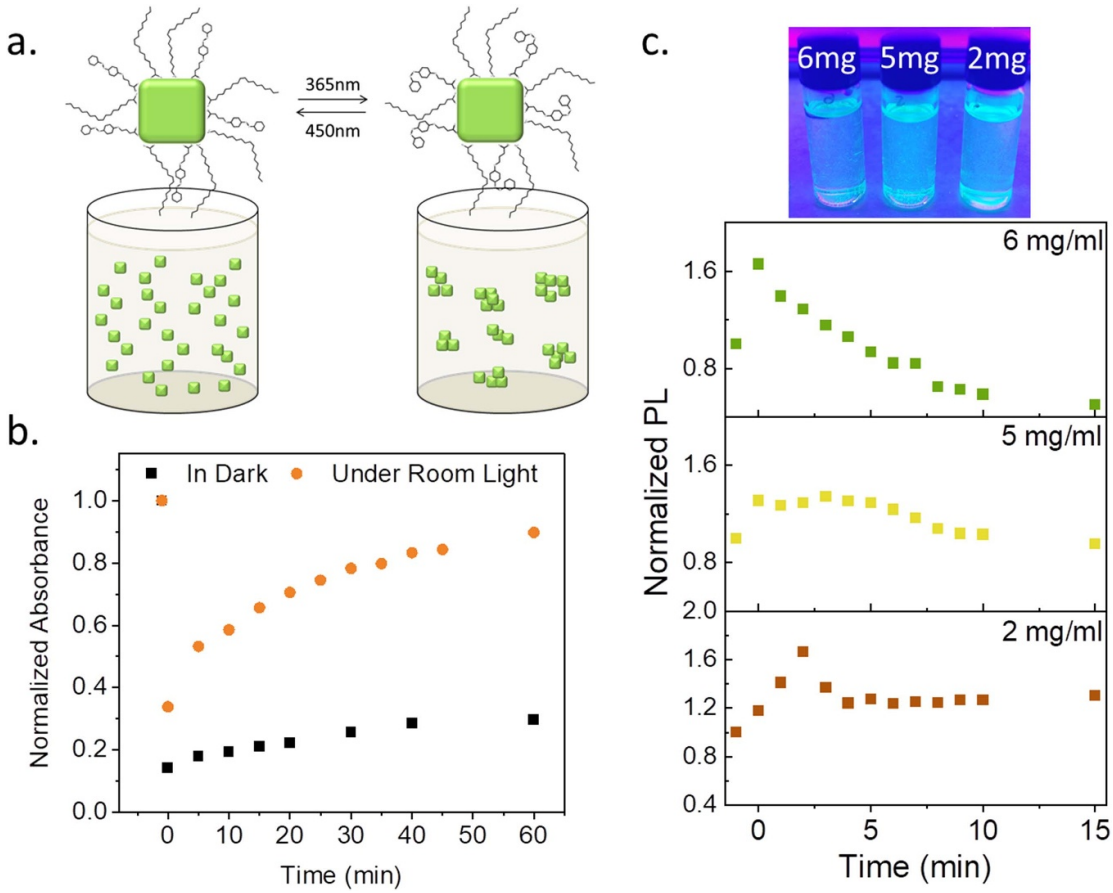

Figure 3. (a) Schematic illustration showing azo ligands coating PeNPs in the solution. The *cis–trans* isomerization is presented based on the excitation wavelength. (b) Normalized absorbance intensity of the ligands at 365 nm with time after exposing the ligands to 365 nm in two conditions; under room light and in dark. (c) Normalized PL intensity as a function of time for PeNPs treated with different concentrations of azo ligands (2, 5, and 6 mg ml^{-1}) and a picture of the solutions under 365 nm (UV) light.

The optical properties of the PeNPs were used to track the changes in the properties of the azo ligands coating the PeNPs. Upon exposure to 365 nm wavelength light, the azo ligands were transferred to the *cis* isomer and turned to polar ligands. These polar ligands that coated the PeNPs started to form aggregates of PeNPs in the nonpolar solvent, which resulted in sedimentation at the bottom of the vial, as illustrated in figure 3(a). The dilution due to sedimentation was reflected in the reduced PL intensity with time, as shown in figure 5S. The thermodynamic stability of the trans isomer induces the transformation of the ligands after exposure to 365 nm from trans to cis. Figure 3(b) follows the isomerization process of the ligands from cis back to trans after exposure to 450 nm. The process was measured under two conditions: dark, and room light. The room light induces the conversion of the cis isomer into trans, then after 60 min the intensity of the trans regain 90% of the initial intensity; while the dark inhibited the isomerization process and only 30% was recovered after 60 min. 30% conversion is not sufficient to halt the aggregation process, hence the PL is decreasing at a period of 60 min (figure 5S). Figure 3(c) shows the effect of ligand concentration (2–6 mg ml^{-1}) on the aggregation. In all concentrations, the PL intensity increased in the first few minutes of 365 nm (UV) illumination starting from $t = 0$. In the case of 2 mg ml^{-1}, the PL intensity increased, and at $t = 3$ min, it decreased, while after $t = 5$ min, it reached a constant PL intensity, suggesting that there were not sufficient ligands to coat all the PeNPs and the aggregation was not sufficient for sedimentation.

In the case of 5 mg ml^{-1} following the first increase in PL intensity, there was no further increase and the PL intensity was constant for the first 5 min. After 5 min, a moderate decrease occurred, which supports our previous assumption in which after 5 min, the process became irreversible as the aggregates were too large and deposited at the bottom of the vial. The 6 mg ml^{-1} concentration had a significant decrease after the first minute of illumination. As the concentration increased, changes in the polarity also increased as a result of the aggregation and sedimentation that formed rapidly, which caused a decrease in the PeNP PL. The image at the top in figure 3(c) shows the aggregates and the color changes of the PeNPs treated with 2, 5, and 6 mg ml^{-1} of ligands. The PL intensity of the 6 mg ml^{-1} concentration was weaker compared with the other concentrations. In addition, we illuminated nontreated PeNPs with 365 nm wavelength light. In this case,

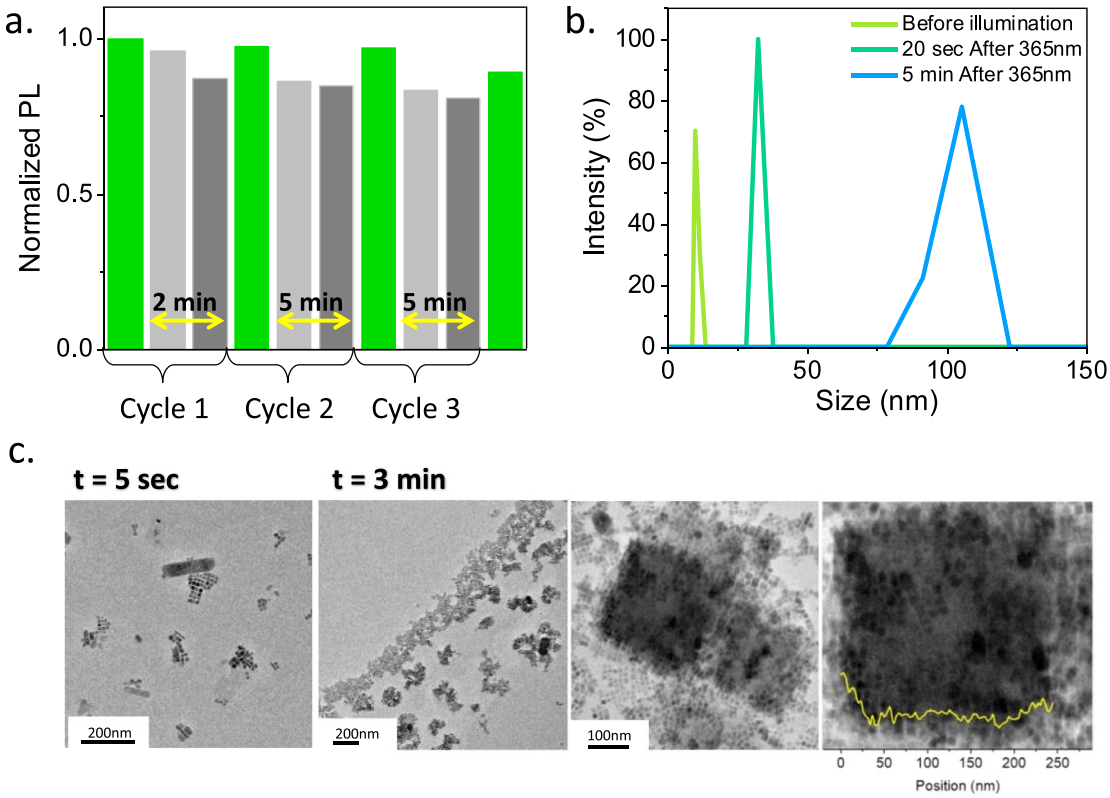

Figure 4. (a) Normalized PL intensity changes of the treated PeNPs before 365 nm illumination (green), immediately after 365 nm illumination (light grey), and 2 or 5 min after 365 nm illumination (dark gray). The next cycle began with 450 nm illumination. The figure shows three cycles. (b) DLS measurements of the PeNPs with time before 365 nm illumination (light green curve) and 20 s (dark green curve) and 5 min (blue curve) after 365 nm wavelength illumination. (c) TEM images of the aggregates formation at 5 s and at 3 min after 365 nm illumination. After 3 min 2D arrays and 3D aggregates are formed. The yellow line shows the transmission along the aggregate.

contrary to figure 3(c), the PL intensity did not show any specific trend; only small fluctuations, which clearly indicated the effect of the azo ligands (see figure 5S).

The next step was to measure the reverse reaction: the disassembly of the PeNP aggregates by exposing them to 450 nm wavelength illumination. Once *cis–trans* isomerization occurred, the PeNPs could disperse again in the nonpolar solvent. We tracked the changes in PL intensity before and after exposure to 365 nm illumination in three cycles. Figure 4(a) shows the normalized PL intensity of the three cycles, where each cycle had: (i) PL before 365 nm illumination (green); (ii) PL immediately after 365 nm illumination (light grey); and (iii) PL 2 or 5 min after 365 nm illumination (dark grey). The next cycle commenced after 450 nm illumination, which is represented by the green bars in the figure. As shown in figure 4(a), PL intensity decreased after exposure to 365 nm illumination, as discussed above. In the first cycle, we exposed the sample to 450 nm wavelength illumination after 2 min, in which the PL intensity almost fully recovered (see the green bar at the beginning of the 2nd cycle in figure 4(a)). In the second cycle, the waiting time was 5 min before the reverse reaction; also, in this case, the PL intensity was very close to the initial PL. However, on the third cycle, the final PL intensity was lower compared with the initial PL, which can be explained by the long waiting time before the reverse reaction. As was shown previously, a longer time was required until sedimentation; therefore, after 5 min, the sedimentation was still moderate, while after an additional cycle (with a waiting time of 5 min), the PL reduction was more pronounced. The reverse reaction was mainly feasible at short waiting times. The TEM images in figure 4(c) show the light-modulated assembly. At 5 s, there were small arrays (less than 100 nm in size) that became larger (up to several hundreds of nm) after 3 min. The images demonstrate the aggregation of small PeNP groups toward large aggregates of PeNPs. In addition to the assembled NPs, after 3 min, we noticed large PeNPs and undefined structures (see figure 6S). We attribute these structures to the irreversible process of the PeNPs reaching their saturation limit. This explains the decrease in the PL intensity at long waiting times (5 min). Measuring the transmission intensity along the aggregate emphasizes the surface roughness which indicates that the surface is composed of separated NPs (figure 4(c)-right). DLS measurements also assisted in tracking the assembly process and in extracting the size of the assembled PeNPs. Figure 4(b) shows that immediately after the exposure to 365 nm

illumination, the detected size of the PeNP aggregates increased from 12 nm to 30 nm, and then to larger sizes after 5 min. The FWHM of the DLS increased after 5 min, which suggests an increase in the size distribution.

4. Conclusions

In this work, we show the use of photoswitchable ligands in $CsPbBr_3$ NPs. H-NMR, DOSY-NMR, absorbance, PL and PM-IRRAS FTIR were used to identify the attachment of the ligands to the surface of the NPs. PL intensity and DLS measurements assisted in tracking the assembly and disassembly processes of these NPs. Upon 365 nm illumination, the PeNPs aggregated; upon 450 nm illumination, the reverse reaction occurred, which was proved for several cycles. This light-controlled, PeNP assembly can be used in advanced inks for 3D printing so that we can utilize the NP properties in the desired product.

Data availability statement

All data that support the findings of this study are included within the article (and any supplementary files).

Acknowledgments

We would like to thank the Israel Science foundation and the Air Force Research Laboratory (AFRL) for their financial support. We would like to thank Iris Berg from Professor Elad Gross' research group for performing the PM-IRRAS measurements.

ORCID iD

Lioz Etgar https://orcid.org/0000-0001-6158-8520

References

[1] Protesescu L, Yakunin S, Bodnarchuk M I, Krieg F, Caputo R, Hendon C H, Yang R X, Walsh A and Kovalenko M V 2015 Nanocrystals of cesium lead halide perovskites ($CsPbX_3$, X = Cl, Br, and I): novel optoelectronic materials showing bright emission with wide color gamut *Nano Lett.* **15** 3692–6
[2] Li G *et al* 2016 Highly efficient perovskite nanocrystal light-emitting diodes enabled by a universal crosslinking method *Adv. Mater.* **28** 3528–34
[3] Tan Y *et al* 2018 Highly Luminescent and stable perovskite nanocrystals with octylphosphonic acid as a ligand for efficient light-emitting diodes *ACS Appl. Mater. Interfaces* **10** 3784–92
[4] Vashishtha P and Halpert J E 2017 Field-driven ion migration and color instability in red-emitting mixed halide perovskite nanocrystal light-emitting diodes *Chem. Mater.* **29** 5965–73
[5] Wang Y, Li X, Nalla V, Zeng H and Sun H 2017 Solution-processed low threshold vertical cavity surface emitting lasers from all-inorganic perovskite nanocrystals *Adv. Funct. Mater.* **27** 1605088
[6] Huang X *et al* 2020 Three-dimensional laser-assisted patterning of blue-emissive metal halide perovskite nanocrystals inside a glass with switchable photoluminescence *ACS Nano* **14** 3150–8
[7] Wu Z *et al* 2021 An excellent impedance-type humidity sensor based on halide perovskite $CsPbBr_3$ nanoparticles for human respiration monitoring *Sens. Actuators* B **337** 129772
[8] Kakavelakis G, Gagaoudakis E, Petridis K, Petromichelaki V, Binas V, Kiriakidis G and Kymakis E 2018 Solution processed $CH_3NH_3PbI_{3-x}Cl_x$ perovskite based self-powered ozone sensing element operated at room temperature *ACS Sensors* **3** 135–42
[9] Hasanzadeh Azar M, Mohammadi M, Rezaei N T, Aynehband S, Shooshtari L, Mohammadpour R and Simchi A 2021 Stable photodetectors based on formamidinium lead iodide quantum well perovskite nanoparticles fabricated with excess organic cations *ACS Appl. Nano Mater.* **4** 7788–99
[10] Liu B, Gutha R R, Kattel B, Alamri M, Gong M, Sadeghi S M, Chan W-L and Wu J Z 2019 Using silver nanoparticles-embedded silica metafilms as substrates to enhance the performance of perovskite photodetectors *ACS Appl. Mater. Interfaces* **11** 32301–9
[11] Pan A, He B, Fan X, Liu Z, Urban J J, Alivisatos A P, He L and Liu Y 2016 Insight into the ligand-mediated synthesis of colloidal $CsPbBr_3$ perovskite nanocrystals: the role of organic acid, base, and cesium precursors *ACS Nano* **10** 7943–54
[12] Udayabhaskararao T, Kazes M, Houben L, Lin H and Oron D 2017 Nucleation, growth, and structural transformations of perovskite nanocrystals *Chem. Mater.* **29** 1302–8
[13] Krieg F *et al* 2018 Colloidal $CsPbX_3$ (X = Cl, Br, I) nanocrystals 2.0: zwitterionic capping ligands for improved durability and stability *ACS Energy Lett.* **3** 641–6
[14] Pan J *et al* 2018 Bidentate ligand-passivated $CsPbI_3$ perovskite nanocrystals for stable near-unity photoluminescence quantum yield and efficient red light-emitting diodes *J. Am. Chem. Soc.* **140** 562–5
[15] Bi C, Kershaw S V, Rogach A L and Tian J 2019 Improved stability and photodetector performance of $CsPbI_3$ perovskite quantum dots by ligand exchange with aminoethanethiol *Adv. Funct. Mater.* **29** 1–9
[16] Kim Y-H *et al* 2020 Strategies to achieve high circularly polarized luminescence from colloidal organic-inorganic hybrid perovskite nanocrystals *ACS Nano* **14** 8816–25
[17] Debnath G H, Georgieva Z N, Bloom B P, Tan S and Waldeck D H 2021 Using post-synthetic ligand modification to imprint chirality onto the electronic states of cesium lead bromide ($CsPbBr_3$) perovskite nanoparticles † *Nanoscale* **13** 15248–56
[18] Li M *et al* 2022 Chiral ligand-induced structural transformation of low-dimensional hybrid perovskite for circularly polarized photodetection *Chem. Mater.* **34** 2955–62
[19] Eastoe J and Vesperinas A 2005 Self-assembly of light-sensitive surfactants *Soft Matter* **1** 338–47

[20] Klajn R, Bishop K J M and Grzybowski B A 2007 Light-controlled self-assembly of reversible and irreversible nanoparticle suprastructures *Proc. Natl Acad. Sci. USA* **104** 10305–9
[21] Raymo F M 2006 Intermolecular Coupling of Motion under Photochemical Control *Angew. Chem. Int. Ed.* **45** 5249–51
[22] Manna D, Udayabhaskararao T, Zhao H and Klajn R 2015 Orthogonal light-induced self-assembly of nanoparticles using differently substituted azobenzenes *Angew. Chem., Int. Ed.* **54** 12394–7
[23] Lawrence R L, Scola B, Li Y, Lim C-K, Liu Y, Prasad P N, Swihart M T and Knecht M R 2016 Remote optically controlled modulation of catalytic properties of nanoparticles through reconfiguration of the inorganic/organic interface *ACS Nano* **10** 9470–7
[24] Wei Y, Han S, Kim J, Soh S and Grzybowski B A 2010 Photoswitchable catalysis mediated by dynamic aggregation of nanoparticles *J. Am. Chem. Soc.* **132** 11018–20
[25] Lawrence R L, Hughes Z E, Cendan V J, Liu Y, Lim C-K, Prasad P N, Swihart M T, Walsh T R and Knecht M R 2018 Optical control of nanoparticle catalysis influenced by photoswitch positioning in hybrid peptide capping ligands *ACS Appl. Mater. Interfaces* **10** 33640–51
[26] Zhao H, Sen S, Udayabhaskararao T, Sawczyk M, Kučanda K, Manna D, Kundu P K, Lee J-W, Král P and Klajn R 2016 Reversible trapping and reaction acceleration within dynamically self-assembling nanoflasks *Nat. Nanotechnol.* **11** 82–88
[27] Neri S, Martin S G, Pezzato C and Prins L J 2017 Photoswitchable catalysis by a nanozyme mediated by a light-sensitive cofactor *J. Am. Chem. Soc.* **139** 1794–7
[28] Zhu L, Yan H, Ang C Y, Nguyen K T, Li M and Zhao Y 2012 Photoswitchable supramolecular catalysis by interparticle host-guest competitive binding *Chem. Eur. J.* **18** 13979–83
[29] Renier O, Bousrez G, Stappert K, Wilk-Kozubek M, Adranno B, Pei H, Spielberg E T, Smetana V and Mudring A-V 2019 Photoisomerization and mesophase formation in azo-ionic liquids *Cryst. Growth Des.* **20** 214–25
[30] Müller M and Zentel R 1993 Azo-dyes as labels and as photoisomerizable units in chiral polyisocyanates *Makromol. Chem.* **194** 101–16
[31] Lednev I K, Ye T Q, Matousek P, Towrie M, Foggi P, Neuwahl F V R, Umapathy S, Hester R E and Moore J N 1998 Femtosecond time-resolved UV-visible absorption spectroscopy of trans-azobenzene: dependence on excitation wavelength *Chem. Phys. Lett.* **290** 68–74
[32] Griffiths J 1972 1. Photochemistry of azobenzene and its derivatives *Chem. Soc. Rev.* **1** 481
[33] Crecca C R and Roitberg A E 2006 Theoretical study of the isomerization mechanism of azobenzene and disubstituted azobenzene derivatives *J. Phys. Chem.* A **110** 8188–203
[34] Udayabhaskararao T *et al* 2018 A mechanistic study of phase transformation in perovskite nanocrystals driven by ligand passivation *Chem. Mater.* **30** 84–93
[35] Liu Z, Bekenstein Y, Ye X, Nguyen S C, Swabeck J, Zhang D, Lee S-T, Yang P, Ma W and Alivisatos A P 2017 Ligand mediated transformation of cesium lead bromide perovskite nanocrystals to lead depleted Cs_4PbBr_6 nanocrystals *J. Am. Chem. Soc.* **139** 5309–12
[36] Wilhelm C and Gardette J L 1994 Infrared identification of carboxylic acids formed in polymer photooxidation *J. Appl. Polym. Sci.* **51** 1411–20